



**BRNO UNIVERSITY OF TECHNOLOGY**

VYSOKÉ UČENÍ TECHNICKÉ V BRNĚ

**FACULTY OF MECHANICAL ENGINEERING**

FAKULTA STROJNÍHO INŽENÝRSTVÍ

**INSTITUTE OF PHYSICAL ENGINEERING**

ÚSTAV FYZIKÁLNÍHO INŽENÝRSTVÍ

# **QUANTITATIVE IMAGING IN SCANNING ELECTRON MICROSCOPE**

KVANTITATIVNÍ ZOBRAZOVÁNÍ V RASTROVACÍM ELEKTRONOVÉM MIKROSKOPU

**SHORT VERSION OF DISSERTATION THESIS**

TEZE DISERTAČNÍ PRÁCE

**PH.D. CANDIDATE**

DOKTORAND

**Ing. Mgr. Radim Skoupý**

**ADVISOR**

ŠKOLITEL

**Ing. Vladislav Krzyžánek, Ph.D.**

**OPPONENT**

OPONENT

**BRNO**

**Date of defense:**

## **KEYWORDS**

low-voltage STEM, SEM, quantitative imaging, qSTEM, qBSE, detector calibration, mass-loss, radiation caused damage, Monte Carlo simulation of electron scattering, coating layer thickness, electron mirror calibration, pixelated STEM detector, 4D STEM, calibration-less qSTEM, local sample thickness, EDX, CL, correlative imaging, cryo-SEM

## **KLÍČOVÁ SLOVA**

nízkonapěťový STEM, SEM, kvantitativní zobrazování, qSTEM, qBSE, kalibrace detektoru, úbytek hmoty, radiační poškození, Monte Carlo simulace elektronového rozptylu, tloušťka krycí vrstvy, kalibrace pomocí elektronového zrcadla, pixelovaný STEM detektor, 4D STEM, bezkalibrační qSTEM, lokální tloušťka vzorku, EDX, CL, korelativní zobrazování, kryo-SEM

## **PLACE OF THESIS MANUSCRIPT STORING**

Department of Science and Research of Faculty of Mechanical Engineering of Brno University of Technology.

© Ing. Mgr. Radim Skoupý

ISBN 80-214-

ISSN 1213-4198

# Contents

<b>Contribution of the thesis</b>	<b>5</b>
<b>Aims of the Thesis</b>	<b>6</b>
<b>1 State of the Art</b>	<b>7</b>
1.1 Quantitative STEM imaging . . . . .	8
1.2 Quantitative BSE imaging . . . . .	10
1.3 Correlation of various signals in SEM . . . . .	11
<b>2 Achieved results</b>	<b>12</b>
2.1 Quantitative imaging using scintillator based STEM detector	12
2.2 Quantitative imaging using annular STEM detector . . . . .	15
2.2.1 Determining the accuracy of qSTEM . . . . .	16
2.2.2 Beam induced mass-loss of embedding epoxy resin . .	17
2.3 Quantitative imaging using pixelated STEM detector . . . . .	18
2.4 Quantitative imaging using annular BSE detector . . . . .	21
2.4.1 Electron mirror calibration . . . . .	21
2.4.2 Mean thickness estimation . . . . .	22
2.4.3 Local thickness mapping . . . . .	23
2.5 Correlation of various signals in SEM . . . . .	25
2.5.1 EDX in combination with SE imaging . . . . .	25
2.5.2 EDX/CL in combination with STEM imaging . . . . .	26
<b>3 Conclusion</b>	<b>27</b>
<b>Bibliography</b>	<b>30</b>
<b>Author's CV</b>	<b>32</b>
<b>Abstract</b>	<b>34</b>



# Contribution of the thesis

The scientific contribution of this doctoral thesis is supported by 22 scientific publications in total. It consists of 7 publications in impacted journals of which 2 of them as the first author, 2 in non-impacted journals and 13 in conference proceedings and abstracts. The core of the thesis are: analysis of accuracy and error sources of quantitative scanning transmission electron microscopy, application of quantitative scanning transmission electron microscopy in epoxy resin mass-loss study and the development of new and innovative methodologies/techniques for quantitative imaging using annular back-scattered electron and pixelated scanning transmission electron microscopy detectors, which were published in high-quality scientific journals. The new approaches may be summarised in following points:

- Epoxy resin sensitivity depends on many conditions, optimal sample preparation and imaging settings may be found and used for suppression of real sample mass-loss caused by electron beam irradiation.
- The use of electron deflection on electron mirror solves a problem with back-scattered electron detector calibration which is situated sensitive side down and just under a pole-piece of final demagnifying lens in a vacuum chamber of a scanning electron microscope.
- The use of pixelated detector of transmitted electrons overcomes a problem with imperfect and drifting calibration values of classical intensity based quantitative scanning transmission electron microscopy technique.

Design activity and development of equipment is documented by two industrial designs, which were used in individual applications. The educational contribution of the thesis is represented by author's co-teaching of the course Physical methods in anthropology (2019; Faculty of Science, Masaryk University), supervising one bachelor student, who successfully defended her work in 2017, consultations for one master student (2016) and reviewer of two bachelor students in 2018. Contribution to the popularisation of science is in author's participation in lectures and excursions within the Brno Days of Electron Microscopy, the Week of Science and Technology and a few workshops within Strategy AV21 of the Czech Academy of Sciences.

# Aims of the Thesis

The classical imaging in the field of electron microscopy brings spatial distribution of imaged physical or chemical properties of a sample without exact information about the amount of this feature. Nowadays, imaging carrying exact information about chosen quantity is becoming more common. Accordingly to this progression from qualitative to quantitative imaging, a wide group of techniques and methods has been developed in last decades.

This thesis deals with the possibilities of quantitative imaging in a scanning (transmission) electron microscope (S|T|EM). There are many combinations of techniques which give information about different chemical, physical or geometrical properties of investigated samples. The aims are divided into separate chapters according to their focus.

- **Scintillator based fully calibrated quantitative STEM detection system** – the detection system is designed as not requiring calibration images and resistant to beam current fluctuation with suppression of associated errors.
- **Quantitative STEM in general** – investigation of accuracy and errors together with its application on EMbed 812 epoxy resin, where sensitivity to irradiation by the primary electron beam accordingly to various conditions is studied.
- **Calibration of retractable back-scattered electron detector** – development of a standardless absolute calibration method, which describes a response of the detector to the electron beam energy and position of an impact.
- **Calibration-less qSTEM using pixelated detector** – thanks to this type of detector, the STEM detector calibration, which is in case of classical qSTEM needed before each imaging session, is not necessary.

The aim of this Ph.D. thesis is methodological development, design, construction and testing of equipment and techniques for quantitative imaging with subsequent proposal of calibration procedures in SEM. The developed methods and procedures are than used in a wide range of applications including the samples from both fields of life and material sciences.

# 1 State of the Art

The field of electron microscopy offers many types of imaging techniques. In general, it is possible to divide all imaging techniques into two groups by dimensionality of the provided information. The first group gives 3D information about the investigated sample. Scanning electron microscopy is represented by techniques using repeated scheme "remove sample and take image", where the remove of sample parts is used in order to expose next parts of a sample. The remove of sample may be performed by focused ion beam milling (FIB-SEM; the technique provides high resolution in  $z$  direction which enables creation of isotropic voxels, but it takes long time and due to that it is suitable for lower sample volumes) or by repeated cutting of a sample by ultramicrotome mounted inside of the microscope chamber (serial block-face imaging; SBF-SEM offers higher investigated volumes but with anisotropic voxels – the size of  $z$  is given by lowest slice thickness possible to cut). In the case of transmission electron microscopy, it is possible to use array tomography, where a sample is cut to series of thin sections and than imaged, stage tilt tomography using the subsequent sample reconstruction from its projections at different angles or single-particle analysis, where identical copies of sample in different orientations are imaged and its 3D structure is computed.

The second group is imaging in 2D. This big group contains a conventional imaging in SEM using a variety of detectors and signals or a planar projection of a sample in TEM and STEM. Quantitative STEM or BSE imaging comes up with a way how to get more quantitative information about the thickness of a sample at each pixel from a single image, but also offers other information about the sample such as a mass per length of filamentous structures, mass per area of sheets, or mass of particles. qSTEM is not the only possibility how to measure the thickness of a sample using transmitted electrons – EELS can be used as well. The difference is in the use of mainly inelastic scattering instead of elastic scattering used in qSTEM [1].

## 1.1 Quantitative STEM imaging

The application area of qSTEM is very wide and consists of different types of samples, imaging strategies and studied features. It can be divided accordingly to the detector type. The annular detector gives information about the amount of electrons impacting the detector in given scattering angle ranges (schematically shown in Fig. 1.1 A). In opposite, the pixelated STEM detector gives a full scattering pattern captured by the rectangular matrix of pixels (shown in Fig. 1.1 B; classical STEM segments like BF, DF and HAADF can be calculated from individual pixelated data).

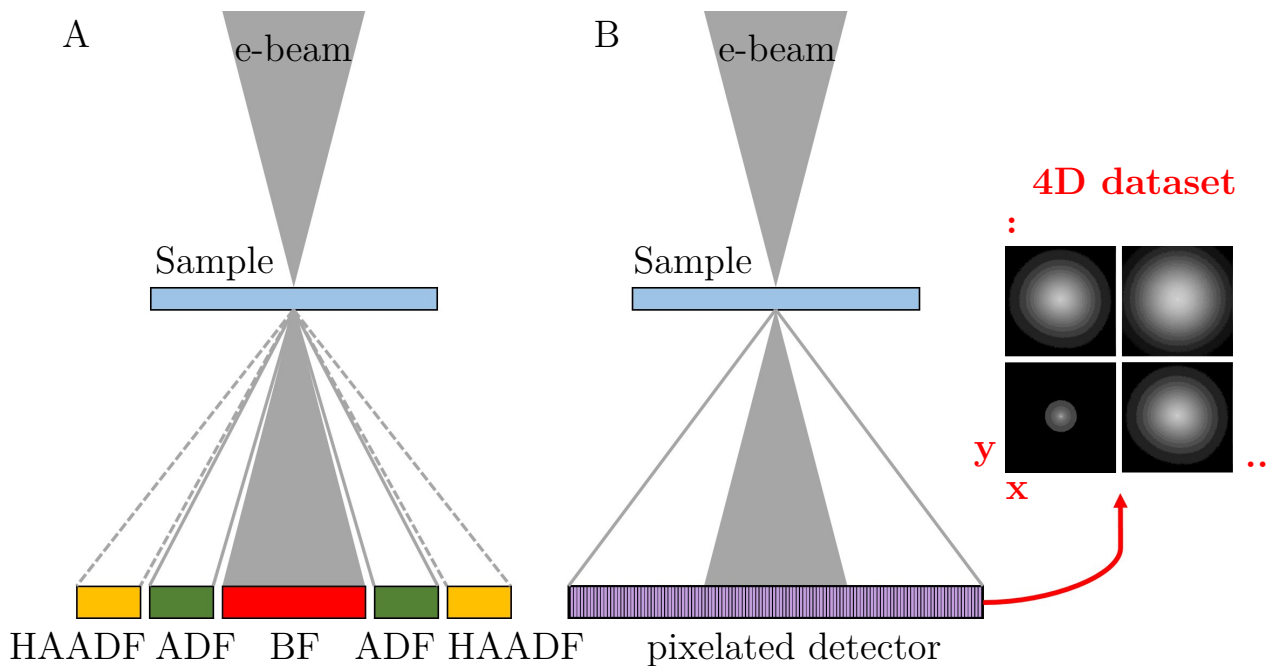


Fig. 1.1: Comparison of annular (A) and pixelated (B) STEM detector.

In a nutshell, the method compares the captured electron intensity normalised between 0 (mean pixel value of the “dark” image) and 1 (mean pixel value of the “bright” image) with a simulated intensity calculated from the number of electrons captured by the detector at a known detection angle and the total number of simulated electrons (principle shown in Fig. 1.2). qSTEM measurement can be done using commercially available detectors. The disadvantage is neglecting of electron beam current changes and the corresponding change of the captured signal.



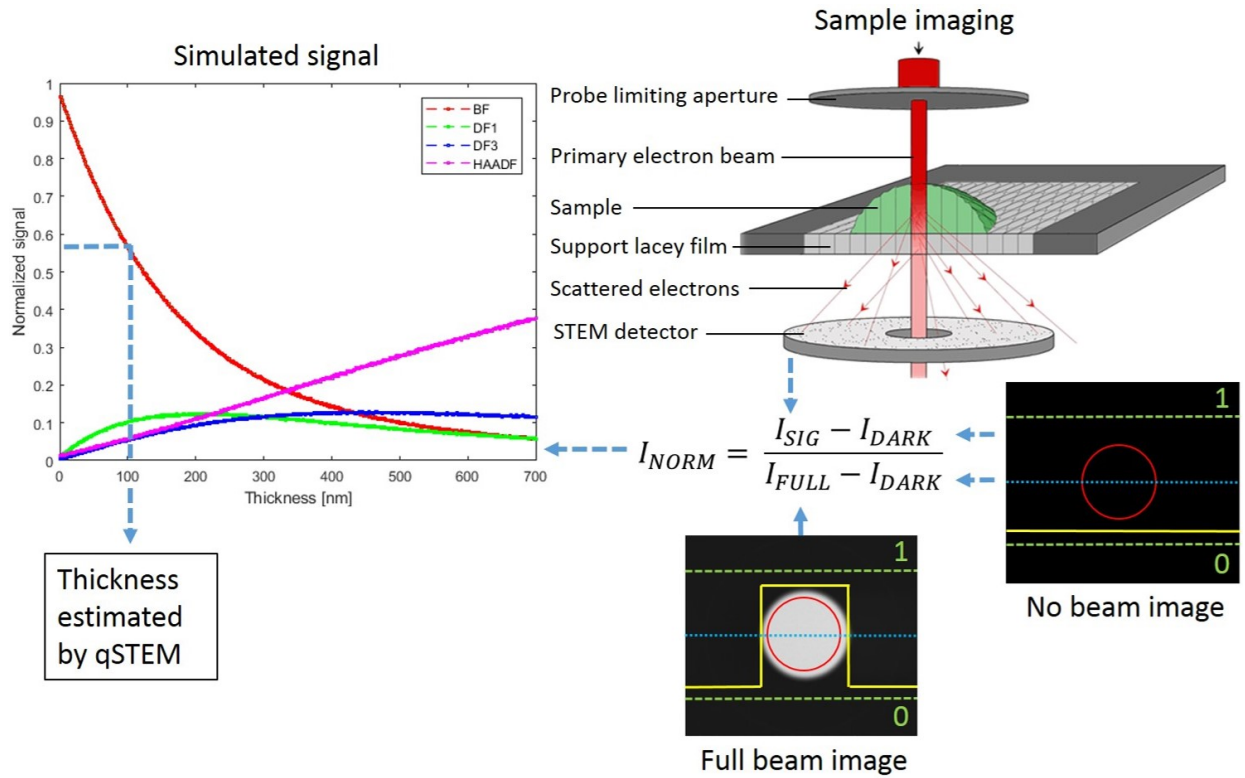


Fig. 1.2: Principle of qSTEM. Electrons scattered by a sample are captured by the detector with known detection angles. The intensity of detected signal normalised accordingly to calibration images (yellow scan shows signal in blue line due to the signal range in green) carries information about mass/thickness of a sample. The resulting thickness is determined by Monte Carlo simulations.

The main assumptions of the method are:

1. Known geometry of the detection system that usually contains the geometry and position of the detector, the sample holder and the pole piece of the final demagnifying lens.
2. Known density and composition of an investigated sample.
3. Linear response of the detector to the electron beam current.

For quantitative measurement, it is necessary to calibrate data before processing them. We used two images captured during each imaging session, one of them for no electrons impacting on the STEM detector, which is shaded by a grid holder (signal in the image is given by brightness settings), and the other for all primary electrons impacting on the STEM detector (which has to be under saturation level). All measured images of real samples are

somewhere between those extreme values. Using this calibration and normalisation of all data to the real probe current in each imaging session, the influence of fluctuations in measurement conditions among individual measurements are eliminated. There are of course other calibration options like a comparison of image intensity at standard samples as used in [2]. As clear from the principle of STEM imaging, the samples are mounted on TEM grids. It depends on the type of the sample if the supporting film is used. It is necessary e.g. for imaging of individual nanoparticles or clusters. On the other hand, standalone sheets may not need any support. It is desirable to use a film as thin as possible with sufficient endurance to the electron beam.

## 1.2 Quantitative BSE imaging

Although qSTEM is an excellent method for measuring the thickness in the nanometer scale, it has one crucial limiting factor. The samples have to be thin enough for penetration by primary electrons. This limits the method for the use on thin films, nanoparticles distributed on the support layer, standalone lamellas etc. It would be appropriate to use a similar concept for thickness coating measurement on substrates. The principle of quantitative BSE imaging is the same as in the case of quantitative STEM. The signal captured by the BSE detector is dependent on several factors such as elemental composition and its corresponding back-scattering coefficient, the local thickness of individual layers or grains, the local density, the energy of the primary electron beam, the collecting angle of the BSE detector and the application of beam deceleration [3, 4, 5]. The maximum measurable layer thickness by qBSE imaging is given by the acceleration voltage and the corresponding penetrability into the sample [6]. Higher acceleration voltage brings a wider measurable range of thicknesses, but with lower modulation of the signal by unit thickness change. It follows that for high-precision with thin layers, the lower acceleration voltage is preferred and, for a high measurable range of thicknesses, higher beam energy should be used as we reported in [7].

## 1.3 Correlation of various signals in SEM

When quantitative information comes from a different detector than from the primarily chosen image, the results can be considered as pseudo quantitative imaging or all-in-one correlative microscopy. There are many combinations in the case of well equipped SEM but unfortunately, no SEM can be equipped with all available techniques. In our lab EDX, CL, SE, BSE, STEM and EBSD detectors are available. Also, the standard sample holders are not suitable for all performed experiments and some new types were developed for special usage.

In the case of EDX analysis on a bulk sample, surface roughness and electric conductivity are very important, because they can influence the resulting accuracy. They can be optimised by polishing and covering the sample with a conductive layer. In the case of a thin sample placed on a TEM grid, there is one more difficulty. The primary electron beam goes through the sample and impacts the stage or bottom part of the vacuum chamber, where additional X-rays are generated. This background limits the quality of acquired spectra. The problem was solved by using a sample holder specially designed to shade the X-ray photons originated under the sample plane.

In the case of CL, placing the sample to the focal point of parabolic collecting mirror of a CL detector plays crucial role. Higher setting accuracy becomes more important in case of weakly emitting samples. Standard TEM grid holder is not applicable because of unsuitable construction, where TEM grids are placed deep under the highest point of the holder. For generation of a sufficient amount of signal higher probe currents may be needed and so lowering sample temperature will be useful.

The developed sample holder assemblies are described in the following documentations (construction part, documentation drawing and some of the main ideas were made by the author of the thesis):

- Cryo-EDX-CL-STEM sample holder is described in functional specimen *Cryo-SEM holder for imaging of thin samples in the transmission mode with elemental and cathodoluminescence analysis.*
- Cryo-CL-SEM is described in functional specimen *Cryo-SEM holder and anticontaminator system for cathodoluminescence analysis in SEM at very low temperatures.*

## 2 Achieved results

### 2.1 Quantitative imaging using scintillator based STEM detector

The developed method of quantitative STEM imaging using home-made detector (model of the detector is shown in Fig. 2.1) is based on simultaneous capturing of an investigated sample image and information about actual probe current (primary beam current is changing, in case of field emission gun, by decreasing of emission current; Fig. 2.2 A).

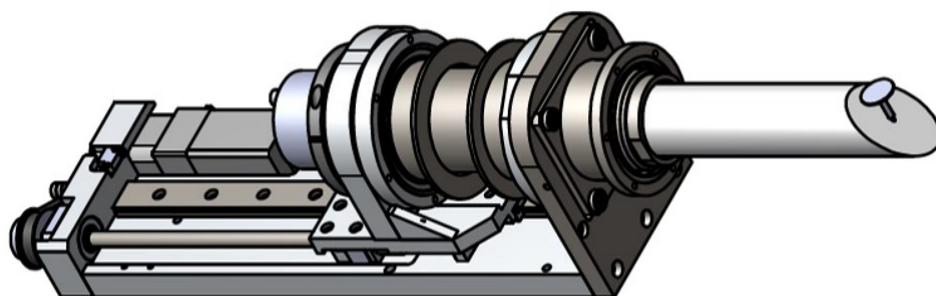


Fig. 2.1: Model of two inch scintillator based STEM detector.

This information can be used for normalisation of the captured data in postprocessing and elimination of the beam current drift caused systematic error. The detector is designed as single electron counting and so very fast and sensitive plastic scintillator was used. This approach has the limitation in the usable probe current range ( $< 2$  pA), because the scintillator is highly beam current sensitive and it is necessary to separate individual light peaks from the scintillator. Construction and manufacturing of mechanical parts of the detector (for the SEM JSM 6700F, JEOL) were done in collaboration with Crytur company (Czech Republic). The calibration process starts with measurement of the actual probe current at different microscope settings by installed Faraday cup. Direct measurement is possible only when the electron probe is focused into the Faraday cup, but not in case of real sample imaging. Actual beam current is monitored by recording the current on the condensor aperture, which is in a constant ratio to the probe current (Fig. 2.2 B).

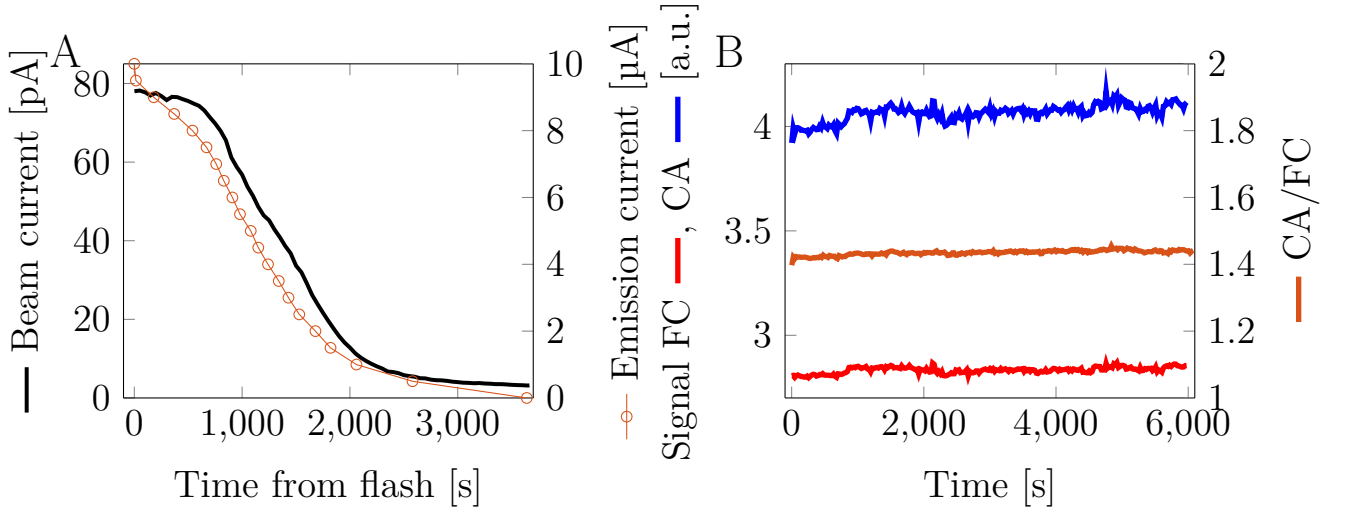


Fig. 2.2: (A) Time dependence of beam and emission current after flash. (B) Long term ratio of condenser aperture (CA) and Farraday cup (FC) measured currents.

Two signals are simultaneously recorded by external scanning unit DISS 5 (Point Electronic, Germany) during the experiment. The first one is digital signal coming from the fast amplifier and discriminator giving the number of electrons in each pixel of the captured image (STEM image). The second one is recording current on the condensor aperture by using the analogue input of the external scanning unit. The signal is converted into the digital image with the same size as the image of investigated sample (the input is calibrated by gain and offset estimation for each analogue preamplifier/channel pair by capturing the signals with known properties provided by a signal generator). The digital intensity in the captured image can be also assigned to specific analogue signal levels and it gives information about time-resolved probe current.

The signal from the photomultiplier tube (R1828-01, Hamamatsu Photonics, Japan) is amplified by a preamplifier and processed using a discriminator. We found an optimal voltage on the photomultiplier, where the signal to noise ratio was measured and its maximum value was chosen. The threshold on the discriminator was estimated from the best signal to noise ratio. Maximum was found in case of detection efficiency of 0.58. The resulting efficiency of 58 % is influenced by a shadow caused by the Farraday cup mounted in the middle of the detector (the detector was slightly pulled out from

the optical axis). The resulting numbers given by the discriminator are then processed by the external scanning unit into an image. Due to the counting of individual electrons, the captured data does not need to be normalised to the detector response when the primary beam is blanked and full primary beam on the detector as it is necessary in the use of non-counting STEM detector. Our detector is in working state and gives satisfactory images at low magnification as demonstrated in Fig. 2.3.

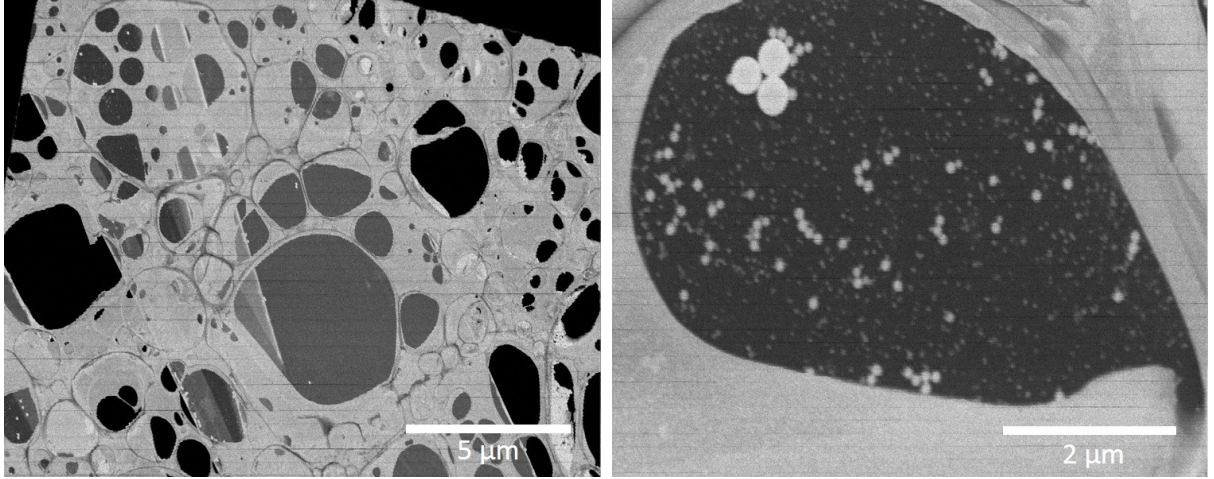


Fig. 2.3: Test sample of latex nanospheres with diameter from 10 up to 400 nm imaged by the home-made STEM detector in low magnification mode.

The images are taken before geometrical calibration of an external scanning unit on a sample with known geometry – TEM grid. The image distortion is visible on non-rectangular shape of grid mesh. The use of the detector for real sample investigation is limited due to complicated primary beam electron trajectories in a magnetic field (captured images are high quality – Fig. 2.4 – but there occurs a problem with Monte Carlo simulations) and the impossibility of magnetic field closure at this type of microscope. We tried to overcome the problem with high magnification mode by using low magnification mode, where no magnetic field is around the sample. Unfortunately, the maximum magnification in this mode is  $10,000\times$ , which is not enough for most of the samples. We used an external scanning unit for finer scanning to obtain images at higher magnifications. Unfortunately, focus control of the microscope is stepping and precise focusing is very time consuming and inaccurate. Due to the above-mentioned issues, the concept



of fully calibrated qSTEM using SEM JEOL JSM 6700F was suspended until solving the problem (either by finding a way how perform alignments in the low-magnification or by closing the field above the sample).

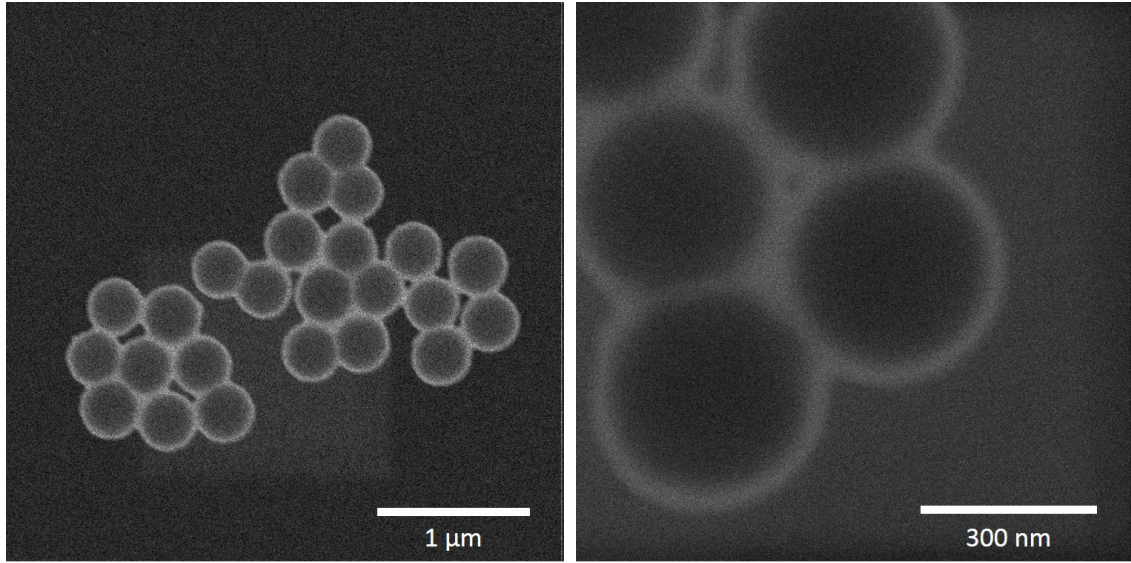


Fig. 2.4: Latex nanospheres with a diameter around 400 nm captured by home-made STEM detector in high-magnification mode.

## 2.2 Quantitative imaging using annular STEM detector

All quantitative imaging using semiconductor annular STEM detector is done with the detector STEM III (FEI - ThermoFisher Scientific, USA) which is divided into seven independent segments (BF, DF1 - DF4 and two HAADF parts as schematically shown in Fig. 2.5). Unfortunately, it is not possible to acquire images from all segments independently and simultaneously, because the SEM Magellan (FEI - ThermoFisher Scientific, USA) is equipped with six independent channels of multipliers and allows only four images to be recorded. The multipliers are not directly assigned to individual segments and they are changing in carousel. Although their characteristics are very similar, some small deviation may occur between them. As the result, the multiplier used for example with BF segment in experiment A can be

different than the multiplier used for BF segment in experiment B. The captured signal would be than different even at the same detector and multiplier settings. At the beginning of each imaging session, it is necessary to choose the segments which carries the most important information about an investigated sample (it is possible to combine individual segments in one window).

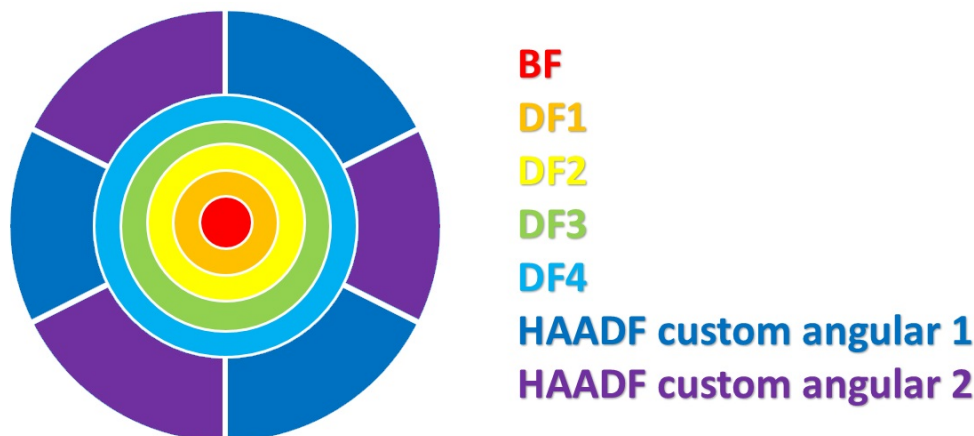


Fig. 2.5: Schematic drawing of STEM III detector segments layout.

### 2.2.1 Determining the accuracy of qSTEM

To compare individual detector segments and their accuracy we used a sample with a known thickness in each point – a latex nanosphere with a nominal diameter of 616 nm. We measured the diameter of 583 nm. The accurate diameter was detected at each particle during the image processing. For the noise limitation and easier comparison of the results, the centre of the nanoparticle is detected and then a rotation averaging is performed. In this step, a distance of each pixel to the centre of the sphere is calculated. Then the pixels with distances in the chosen range are averaged. The advantage of this method is the absence of the interpolation error. However, a small amount of pixels in the middle of the particle causes significantly higher inaccuracy given by higher noise influence. Unfortunately, not all used segments gave us the same results. Both BF and HAADF segments brought results which corresponded very well with the character of the sample with maximum error around 10%. BF showed a little bit higher, and HAADF brought a little bit lower thicknesses than those given



by the geometry of the sample. However, it is possible to improve the accuracy of the method by averaging the curves. In case of the "mean" curve, the accuracy is better than 2% in nearly all examined ranges of thicknesses. High errors (shown in Fig. 2.6) in the range of thicknesses under 100 nm are caused by inaccurate detection of a nanosphere diameter, imperfect spherical shape and wedge shape MC simulation body.

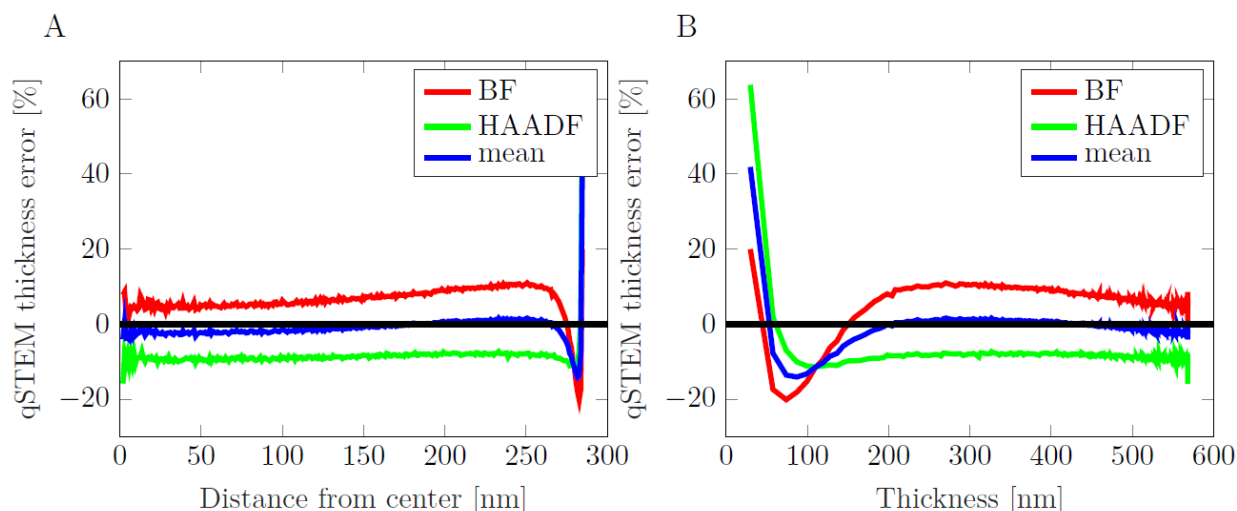


Fig. 2.6: Relative qSTEM thickness error dependency on the distance from the particle centre (A) and on the local geometrical thickness (B).

## 2.2.2 Beam induced mass-loss of embedding epoxy resin

qSTEM was used in the examination of epoxy resin EMbed 812 (Electron Microscopy Sciences, USA) and their properties under the electron beam. The study was done in collaboration with Laboratory of electron microscopy of the Biology Center of the Academy of Sciences in České Budějovice, where preparation, slicing and mounting of the thin slices on the TEM grids was done. We focused on several factors (ageing, carbon layer coating, beam current, staining, plasma cleaning and temperature) which can have an influence on the stability of the sections under electron beam and on the quality of the images of samples embedded in this type of resin respectively. More details can be found in R. Skoupy, J. Nebesarova, M. Slouf, and V. Krzyzanek. Ultramicroscopy Quantitative STEM imaging of electron beam induced mass loss of epoxy resin sections. *Ultramicroscopy*, 202(March):44–50, 2019. doi:10.1016/j.ultramicro.2019.03.018.

## 2.3 Quantitative imaging using pixelated STEM detector

The disadvantage of classical qSTEM is the need to calibrate the detector before the actual measurement. This makes impossible to use images that were taken with contrast and brightness setting adequate for imaging (using the whole range from black to white). We present a method how this disadvantage can be overcome and thickness evaluation can be performed even in the case of non-calibrated images. **The qSTEM changes to calibration-free with the use of 2D pixelated STEM detector.** Just setting to avoid under and over-saturation is needed. The method is based on a change of position of the maximum signal peak on the detector accordingly to sample thickness.

Regular qSTEM technique uses detector calibration process as a bridge between a captured image of a sample and a computer simulation of electron scattering in a model sample with known geometry and composition [8, 9]. Unfortunately, this approach needs the capturing of two calibration images before each imaging session and it is probe current, beam energy and contrast/brightness dependent. We present a simple method for quantitative imaging using 2D STEM pixelated detector. In this case, no special calibration is needed. 4D datasets captured by the 2D STEM detectors are often used for many imaging and analytical techniques including thickness measurement in the field of material science and diffracting samples [10] or less frequently used for the analysis of amorphous samples [11]. The presented 4D-qSTEM method is based on shifting of the most common scattering angle to the higher angles with increasing sample thickness. As the primary electron beam is scanned over the sample (Fig. 2.7 A, B), individual scattering maps are captured for each beam position (Fig. 2.7 D). Individual pixels are summarised by their distance from the centre (it is not rotational average but the sum of pixels at the same angle; Fig. 2.7 C) and plotted accordingly to its angle based on the detector/sample geometry (Fig. 2.7 E).

The computational inputs of the method are similar dependencies based on the Monte Carlo simulation of the electron scattering in a sample with known thickness, density and composition. The most probable scattering

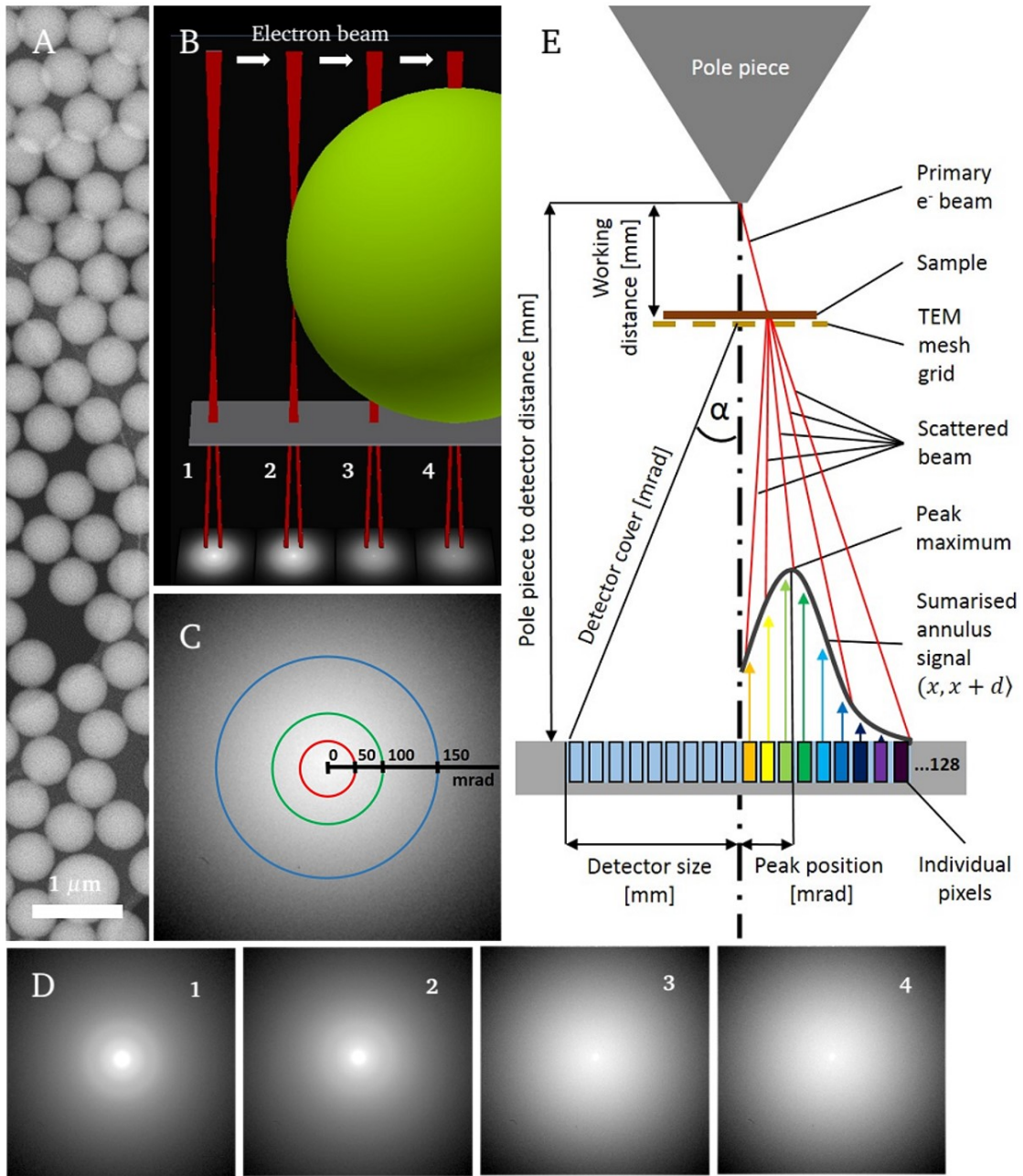


Fig. 2.7: Schematic drawing of 4D-qSTEM method. (A) Test sample of latex nanospheres. (B) Electron beam scans over a sample and scattering pattern is captured for each beam position. (C) Highlighting of pixels with the same chosen scattering angles. (D) Scattering patterns in beam positions 1-4. (E) Principle of calibration-less qSTEM imaging. Amount of electrons captured by individual pixels is summarised accordingly to its position on detector – angular deviation from optical axis with the vertex in the plane of the sample. Peak position of summarised annulus signal in mrad carries information about local thickness/density/composition.

angle is found at both parts and local thickness is estimated by finding the experiment-based angle in simulation-based series.

In the first experiments, latex nanospheres with a diameter of 575 nm (Fig. 2.8 A) were chosen as a model sample for their well-known dimensions in every point. From the comparison of the experimental scattering angle dependency and the simulation, the best match was found for the thickness 555 nm (Fig. 2.8 B). The error of estimation is around 3.5 % according to the measured nanosphere diameter, but this error could be caused by the imperfectly round shape of the nanosphere.

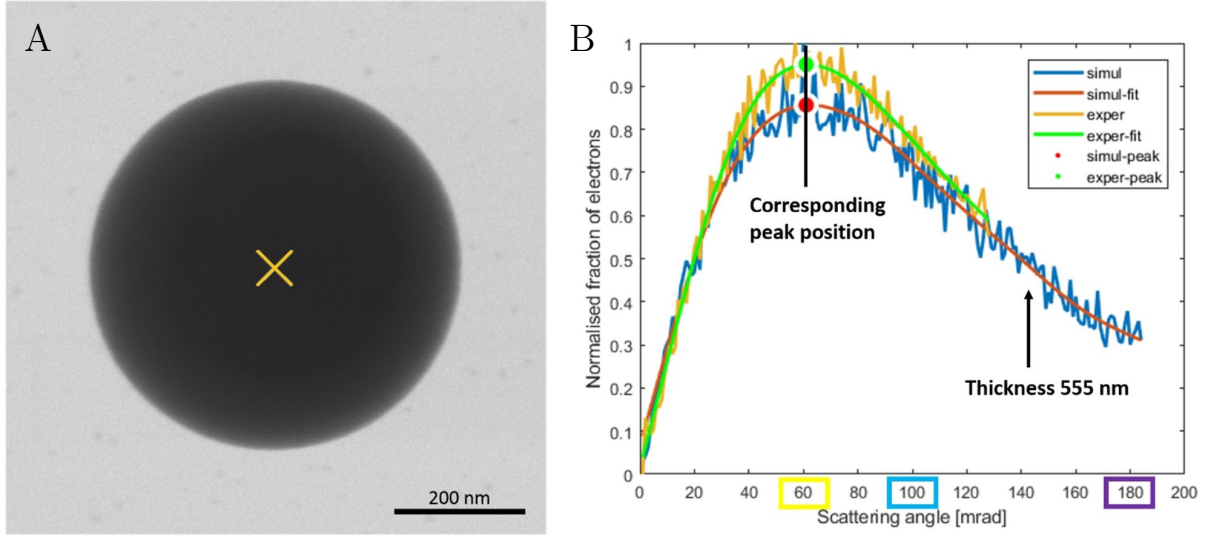


Fig. 2.8: (A) Test sample of a latex nanosphere with a diameter of 575 nm with the measured point in the middle of the sphere. (B) Comparison of scattering angle dependencies from the measured point and simulation for 555 nm thick layer of latex. Position of both peaks is at 61 mrad.

The main advantage of the method is that no previous detector calibration is needed. The usable range of the thicknesses, which can be determined, is given by the creation of detectable peak at low scattering angles for low thicknesses. In the case of latex, the measurable range is from 185 to 1000 nm. We assume that this method can enrich a number of methods based on pixelated STEM detectors and extend their use on amorphous types of samples.

## 2.4 Quantitative imaging using annular BSE detector

The technique of quantitative imaging as described for STEM is usable for BSE detectors as well, but there occurs a problem with precise calibration and response measurement of the BSE detector due to its position in SEM chamber because primary electrons cannot hit the BSE detector directly as in the case of STEM detector (Fig. 2.9 A). The most of the studies use a comparison of a captured image with an image of known standard sample for its normalisation.

### 2.4.1 Electron mirror calibration

We present a simple method for standard-less BSE detector calibration, which together with Monte Carlo simulation of BSE signal emitted from a sample with given geometry, brings a straight forward methodology of thin cover layer thickness measurement on substrates. The inability to irradiate the BSE detector by primary electron beam directly is overcome by the application of the electron mirror for reversion of electron trajectories as shown in Fig. 2.9 B.

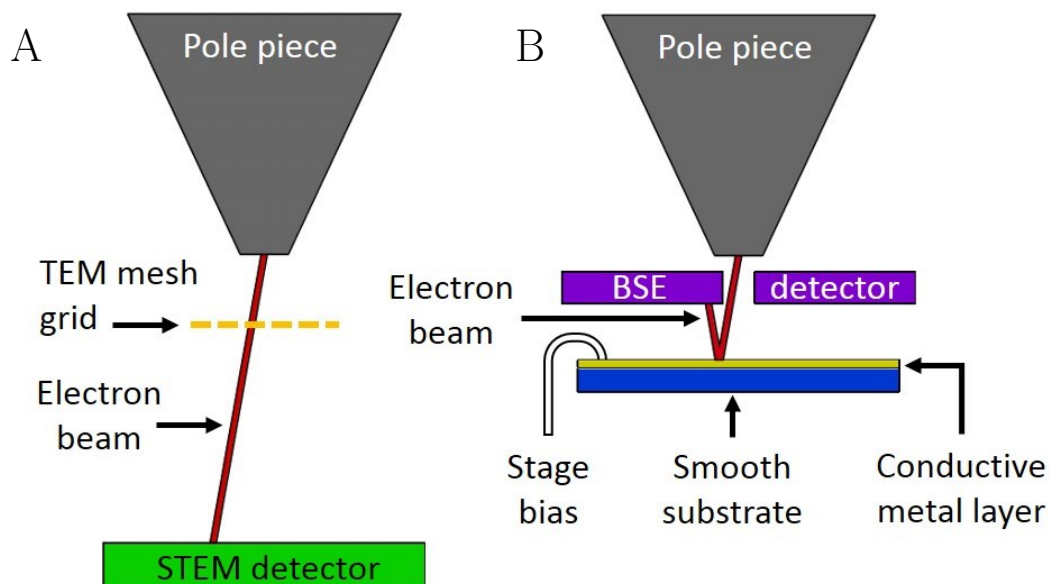


Fig. 2.9: Diagram of energy-dependent calibration of STEM detector (A) and BSE detector (B). Taken from [12].

We tried several types of biased mirror samples (mica, Si wafer and glass) and the best results we obtained with gold-covered microscopy cover glass. Resulting selfie image of the BSE detector gives detector response to the full beam which is used as the upper limit for data normalisation of real sample images. The Fig. 2.10 shows reversed calibration images of the BSE detector. The bottom limit is obtained from the image captured by the BSE detector when the electron beam is blanked. It is important to take care of over/undersaturation during the image recording.

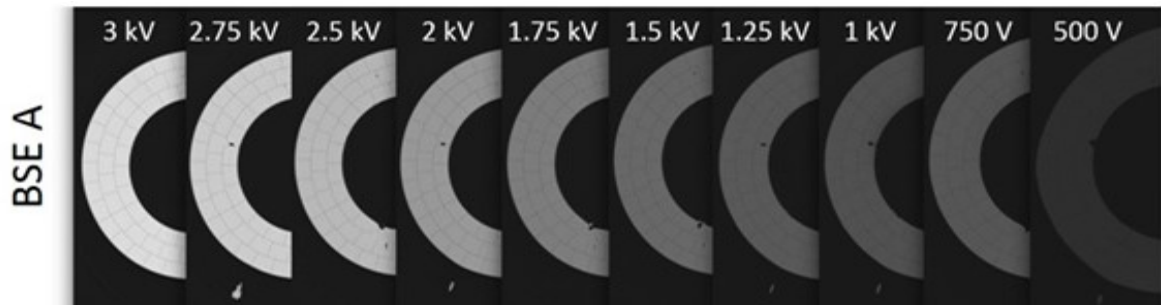


Fig. 2.10: Dependence of pixel intensity of the inner BSE detector segment A on beam energy. Contrast/brightness settings were the same across all energies. Adapted from [12].

## 2.4.2 Mean thickness estimation

We proved this method on a series of samples with different composition (Cr, Mo, Au) and thicknesses. In case of Cr and Mo the range was from 1 up to 25 nm and from 1 up to 13 nm in case of Au. All samples were prepared by calibrated sputtering on a silicon wafer as the substrate. We found a high precision of estimation with an error lower than 20 % in most cases (Fig. 2.11). We assume that real error is different because of the inaccuracy of thickness determination by measuring the sputtering time. The great advantage of this method is its magnification independence in a wide range from a hundred to several hundred thousand times. For more detailed results of the study see the paper R. Skoupy, T. Fort, and V. Krzyzanek. Nanoscale Estimation of Coating Thickness on Substrates via Standardless BSE Detector Calibration. *Nanomaterials*, 10(2):332, 2 2020. doi:10.3390/nano10020332.



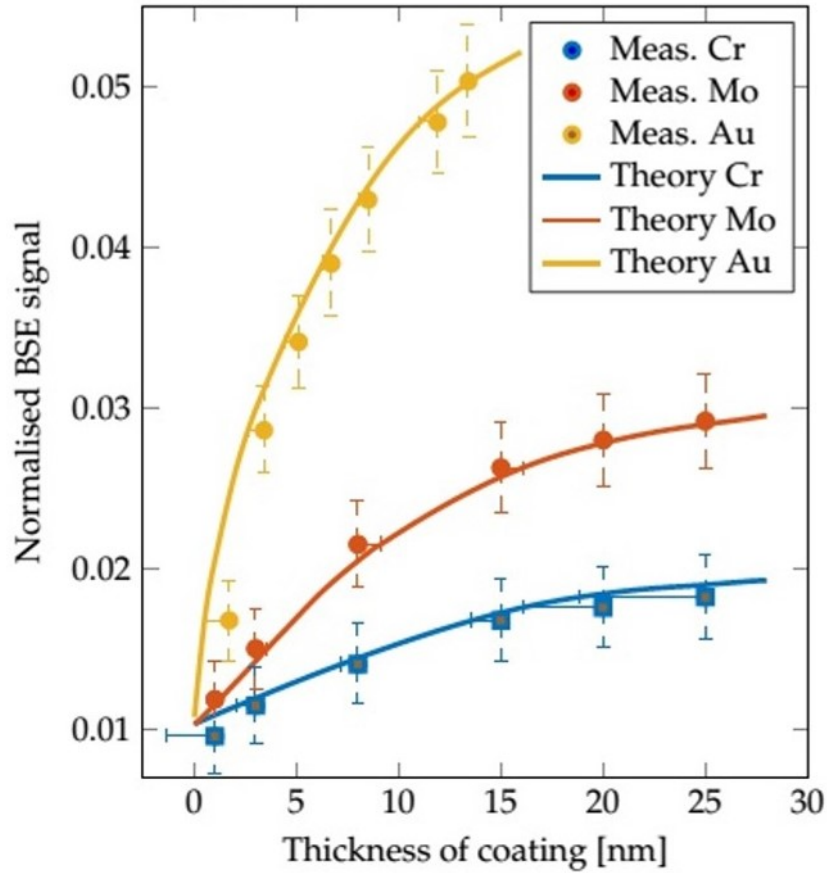


Fig. 2.11: Results of qBSE imaging – comparison of measured and nominal thicknesses. Most of the measurements show an error lower than 1.2 nm or 20 %. Theoretical BSE signal captured by A segment in working distance of 4 mm for Cr, Mo and Au. The individual points show mean values of measured samples with its standard deviation and horizontal lines indicates the thickness assigned by qBSE imaging. The oxidised layer of Cr is highlighted by square marks. Adapted from [7].

### 2.4.3 Local thickness mapping

The results of coating layer thickness mapping on a sample of 25 nm Mo on Si substrate is shown in Fig. 2.12. Areas of different coating layer thickness were found after appropriate data filtering. The mean value of 25.45 nm corresponds with its nominal thickness of 25 nm. It is evident from these results, that for higher resolution the image magnification has to be increased. The use of individual pixel values or just light filtration brings significant errors.

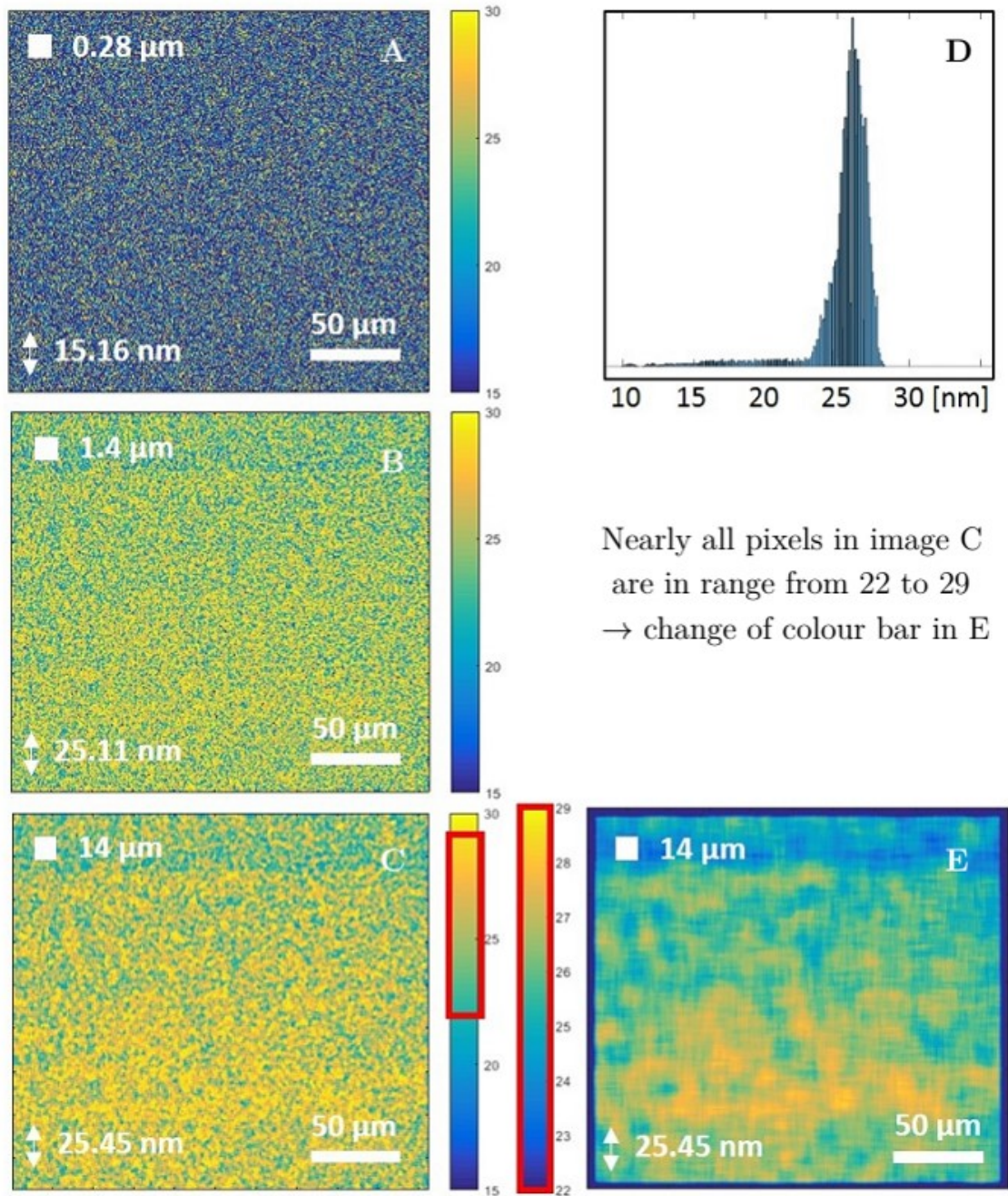


Fig. 2.12: Results of qBSE thickness mapping of the Mo layer with a nominal thickness of 25 nm. (A) Data without filtering – high influence of noise. (B) The same data after 2D median filtration with window  $5 \times 5$ . (C) The same data after 2D median filtration with window  $50 \times 50$ . (D) Histogram of values from image part C. (E) Resulting map shows thicker region in the lower part of an investigated area. Each map has information about the size of filter window  $\square$  and mean estimated thickness  $\updownarrow$ .



## 2.5 Correlation of various signals in SEM

### 2.5.1 EDX in combination with SE imaging

The great potential of EDX-SEM is in the detection of unusual chemical elements included in ancient human dental calculus to verify the hypotheses about life and burial habits of ancient populations and individuals. Analyses were performed on archaeological samples of three chosen individuals from different time periods. The unusual presence of Mg, Al, and Si in the first sample could confirm the hypothesis of high degree of dental abrasion caused by particles from grinding stones in flour. In the second sample, the presence of Cu could confirm that bronze jewelry could lie near the buried body. The elemental composition of the third sample with the presence of Pb and Cu confirms the origin of individual to Napoleonic Wars because the damage to his teeth could be explained by the systematic utilization of the teeth for the opening of paper cartridges (a charge with a dose of gun-powder and a bullet), which were used during the 18th and the 19th century AD. All these results contribute to the reconstruction of life and burial habits of ancient populations and individuals [13]. The main findings are summarised in Fig. 2.13.

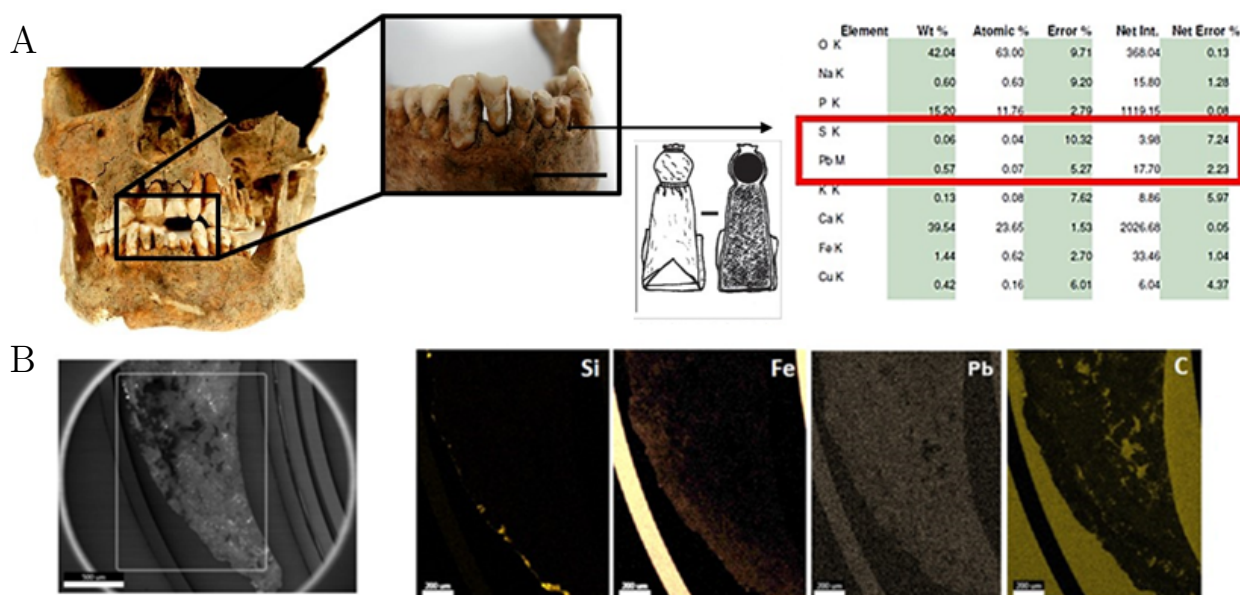


Fig. 2.13: (A) Presence of Pb/S and Cu in the tartar EDX spectrum. Bar 10 mm. (B) EDX map of tartar cross-section. Bar 0.5 mm.

## 2.5.2 EDX/CL in combination with STEM imaging

In the presented study, biokinetics and deposition of titanium dioxide nanoparticles were studied in female ICR mice, after continuous 12-week exposure in inhalation chamber. Uniformity, shape and size of NPs were characterized by TEM and SEM. The study particularly focused on the distribution of Ti NPs in selected tissues. The samples of lung, liver, kidney, spleen and brain were sectioned, fixed and then embedded in Epon–Durcupan mixture. TEM and/or SEM were used for sample observation. Finally, EDX was used in order to evaluate Ti presence in secondary lysosomes of target organ cells. The results indicate that Ti NPs may pass into alveoli and then passively transfer through their membrane, as no signs of phagocytosis or endocytosis were observed. The exposure to Ti NPs gradually induced a loss of type I pneumocytes and alveoli thickening. Within the type II pneumocytes, Ti NPs were found to be deposited within secondary lysosomes, as confirmed by two types of independent EDX analyses. In general, our findings seem to support the hypothesis that the inhaled Ti NPs are translocated via lung-red blood cells-target organ axis and that erythrocytes may serve as principle carriers of Ti NPs [14]. The main findings are summarised in Fig. 2.14.

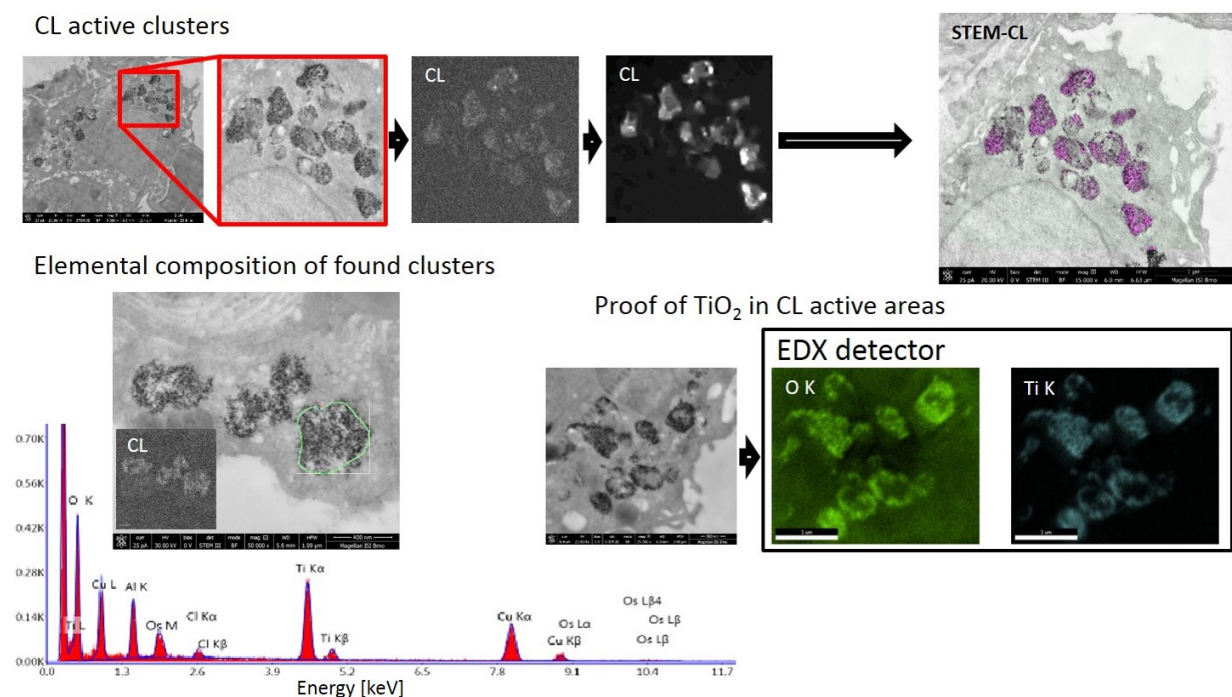


Fig. 2.14: Correlative imaging of TiO<sub>2</sub> NPs inside lung mouse tissue.

### 3 Conclusion

The presented thesis describes the possibilities of quantitative imaging in SEM. The thesis includes necessary theory description in the *Part I: State of the Art*. The main focus is placed on types of signals generated in SEM after impact of primary electron beam and their using in various imaging and analytical techniques. It also gives overview of electron beam/matter simulation principles and software, which are available and widely used in the field of electron microscopy. The theoretical part consists of basic description of fundamental processes, physics and techniques with links to closely focused literature dealing with individual areas, where very detailed descriptions can be found. This part is composed of information from literature review or web pages dealing with Monte Carlo software and summarises available knowledge.

Previous purely theoretical part is followed by the *Part II: Quantitative imaging* which is based on recently published literature review together with author's findings, simulations and experience added with the aim to ensure easier understanding and clarity. The methods of quantitative STEM and BSE imaging are introduced and described in detail. It includes principles, application areas, specifics of different detector types (scintillator based vs. semiconductor, annular vs. pixelated), detector calibration methods and their influence on the results or signal transformation from qualitative to quantitative. Moreover two quantitative imaging modes: *thickness measurement assuming a constant density* and *density measurement assuming a constant thickness* are introduced and discussed for further use in the application part.

The most comprehensive *Part III: Results* shows achieved results, which were accomplished during work on the thesis. The description is in very detailed form in case of results, which were not published in reviewed journals yet. On the other hand, the results that have been so far published are mentioned only in the form of an overview with highlighting of the main ideas together with links to the full texts placed in the annexes. This part is divided into several chapters which differ in their focus. The first one, *Chapter: Quantitative imaging using scintillator based STEM detector* represents fully calibrated detection system for qSTEM. The system has its main ad-

vantage in simultaneous beam current fluctuation correction during the data acquisition. The system was mounted, tested and prepared for its use in applications when a previously unexpected problem has occurred. The system is working in low-magnification mode where no magnetic field is on a sample, but for practical use the maximum magnification of low-mag mode is not satisfactory. Unfortunately, the magnetic field closure is not provided for this type of microscope and the effort to bypass the limitation by refining the scan step with external scanning unit brought interference to the captured image. The experiences gained during the system development were used during design of second generation of fast scintillator based STEM detector, which is adapted for its mounting on more suitable microscopes. The next *Chapter: Quantitative imaging using semiconductor annular STEM detector* deals with in-depth analysis of the accuracy of the method and influence of imperfect STEM detector adjustment on the optical axis of the electron column. It was found out, that usual misalignment does not bring any significant errors and no special care is needed. The accuracy was estimated on sample of latex nanosphere where true local thickness can be computed from its geometry. The error was estimated in percent units for individual STEM detector segments with possible accuracy enhancing, by simultaneous imaging in two different segments (BF and HAADF). The method of qSTEM was applied for the study of electron beam induced mass-loss of epoxy resin sections at various conditions. The aim was to find out recommendations which would reduce the induced mass-loss. The samples of EMbed 812 resin were studied in slices with thicknesses of 30, 60, 100 and 150 nm and beam energy of 30 keV. The variable conditions were age, staining, beam current, plasma cleaning, covering by thin carbon layer and temperature. The general recommendation coming from our study is imaging around the day 10 after slicing, cover slices by a thin carbon layer, work without staining and plasma cleaning and at low temperatures. Beam current dependency is weak and do not play significant role. The main disadvantage of annular STEM detector based qSTEM is its need for a precise detector calibration and contrast and brightness settings before each imaging session. This limitation may be overcome by using different signal property than the signal intensity. The *Chapter: Quantitative imaging using pixelated STEM detector* presents

a new methodology of calibration-less quantitative STEM imaging. In this case, the angle of the most probable scattering is used instead of image intensity and so contrast drift does not play any role. This approach has limitation in finite range of thicknesses which can be measured. It is given by a creation of detectable peak in amount of captured electrons to angle dependency and maximum cover angle of the detector. Another advantage of the method is the possibility to apply it on previously captured data because no special steps are needed before imaging. The principle of quantitative imaging is not limited to STEM detector and it is applicable for BSE detector as well. Many papers dealing with quantitative BSE imaging can be found, but all of them use some type of standard based calibration for linking captured data and simulation or standard series. The *Chapter: Quantitative imaging using BSE detector* introduces new BSE detector calibration technique, which enables absolute and standard-less calibration of the detector in its working (inserted) position. The primary electron beam is reflected on biased electron mirror, made of thin gold coating on a glass substrate, and impacts the detector on its sensitive side. The developed calibration method was proved by measurement of thin metal coatings on silicon substrates with high accuracy better than 1 nm in most cases. The qBSE technique is magnification independent in wide range of magnifications (tested from 50 up to  $500,000\times$ ) and the information about local covering layer thickness is in each pixel of the captured image and thus the method is applicable for 2D mapping at various fields of view.

Last but not least, the thesis includes multiple applications of widespread quantitative techniques of cathodoluminescence and energy dispersive X-ray spectroscopy in combination with high resolution imaging in transmitted or secondary electrons. The *Chapter: Correlation of various signals in SEM* consists of five different applications dealing with different types of samples. To perform those measurements several types of sample holders enabling correlative CL, EDX and STEM/SE were designed, made and applied.

In general, the thesis presents the possibilities of quantitative imaging in scanning electron microscope together with instrumental and methodological development of 2D-STEM and BSE detector based techniques, where significant results and improvements were achieved.

# Bibliography

- [1] M. Tian, O. Dyck, J. Ge, and G. Duscher. Measuring the areal density of nanomaterials by electron energy-loss spectroscopy. *Ultramicroscopy*, 196(March 2018):154–160, 1 2019. doi:10.1016/j.ultramicro.2018.10.009.
- [2] V. Morandi and P. G. Merli. Contrast and resolution versus specimen thickness in low energy scanning transmission electron microscopy. *Journal of Applied Physics*, 101(11), 2007. doi:10.1063/1.2745333.
- [3] A. M. D. Assa’d and M. M. E. Gomati. Backscattering Coefficients for Low Energy Electrons. *Scanning Microscopy*, 12(1):185–192, 1998.
- [4] W.-R. Lin, Y.-J. Chuang, C.-H. Lee, F.-G. Tseng, and F.-R. Chen. Fabrication and characterization of a sensitivity multi-annular backscattered electron detector for desktop SEM. *Sensors*, 18(3093):1–13, 2018. doi:10.1109/ISNE.2018.8394642.
- [5] V. Krzyzanek, N. Sporenberg, U. Keller, J. Guddorf, R. Reichelt, and M. Schönhoff. Polyelectrolyte multilayer capsules: Nanostructure and visualisation of nanopores in the wall. *Soft Matter*, 7(15):7034–7041, 2011. doi:10.1039/c1sm05406f.
- [6] J. Seiter, E. Müller, H. Blank, H. Gehrke, D. Marko, and D. Gerthsen. Backscattered electron SEM imaging of cells and determination of the information depth. *Journal of Microscopy*, 254(2):75–83, 2014. doi:10.1111/jmi.12120.
- [7] R. Skoupy, T. Fort, and V. Krzyzanek. Nanoscale Estimation of Coating Thickness on Substrates via Standardless BSE Detector Calibration. *Nanomaterials*, 10(2):332, 2 2020. doi:10.3390/nano10020332.
- [8] R. Skoupy, J. Nebesarova, M. Slouf, and V. Krzyzanek. Ultramicroscopy Quantitative STEM imaging of electron beam induced mass loss of epoxy resin sections. *Ultramicroscopy*, 202(March):44–50, 2019. doi:10.1016/j.ultramicro.2019.03.018.







- [9] M. Pfaff, E. Müller, M. F. G. Klein, A. Colsmann, U. Lemmer, V. Krzyzanek, R. Reichelt, and D. Gerthsen. Low-energy electron scattering in carbon-based materials analyzed by scanning transmission electron microscopy and its application to sample thickness determination. *Journal of Microscopy*, 243(1):31–39, 2011. doi:10.1111/j.1365-2818.2010.03475.x.
- [10] C. Ophus. Four-Dimensional Scanning Transmission Electron Microscopy (4D-STEM): From Scanning Nanodiffraction to Ptychography and Beyond. *Microscopy and Microanalysis*, 25(3):563–582, 6 2019. doi:10.1017/S1431927619000497.
- [11] X. Mu, A. Mazilkin, C. Sprau, A. Colsmann, and C. Kübel. Mapping structure and morphology of amorphous organic thin films by 4D-STEM pair distribution function analysis. *Microscopy*, 68(4):301–309, 2019. doi:10.1093/jmicro/dfz015.
- [12] R. Skoupy and V. Krzyzanek. Beam energy dependent calibration of STEM and BSE detectors for thin film thickness estimation. In *Microscopy and Microanalysis, Milwaukee*, Milwaukee, 2020.
- [13] D. Fialova, R. Skoupy, E. Drozdova, A. Patak, J. Pinos, L. Sin, R. Benus, and B. Klima. The Application of Scanning Electron Microscopy with Energy-Dispersive X-Ray Spectroscopy (SEM-EDX) in Ancient Dental Calculus for the Reconstruction of Human Habits. *Microscopy and Microanalysis*, 23(6):1207–1213, 2017. doi:10.1017/s1431927617012661.
- [14] M. Machala, P. Kulich, O. Sery, S. Marvanova, R. Skoupy, A. Rusnak, P. Mikuska, and Z. Vecera. The deposition of inhaled titanium nanoparticles in mice organs. In *Toxicology Letters: Abstracts of the 52nd Congress of the European Societies of Toxicology (EUROTOX) Fibes Congress Center Seville*, volume 258, page S277, 2016. doi:10.1016/j.toxlet.2016.06.1969.






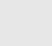
# Author's CV Working Experience

## Radim Skoupy



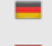

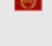

Ph.D. student

-  **Date of Birth:** Jan. 31, 1989
-  Brno, Czech Republic
-  +420 733-320512
-  skoupy.radim [at] gmail.com
-  <http://isibrno.cz/en/microscopy-biomedicine>
-  ORCID: 0000-0003-0665-3873

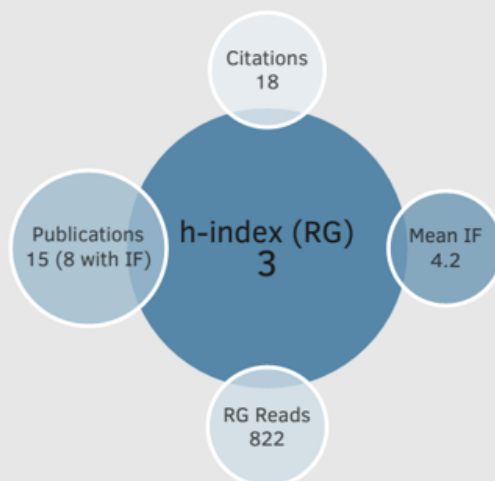
## Areas

-  Cryo-SEM
-  FIB-SEM
-  Correlative Imaging
-  Quantitative Imaging
-  Monte Carlo Simulations
-  BSE, STEM, CL, EDX

## Languages

-  Czech 
-  English 
-  German 
-  Latin 


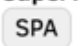
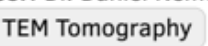
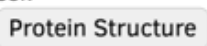
## Metrics



- Sep, 2014 – ongoing **Ph.D. Student** **Institute of Scientific Instruments of the CAS, Czechia**  
Working as a PhD student in group of Microscopy for Biomedicine. Major research area includes quantitative imaging in a SEM together with correlative imaging.
- Oct, 2019 – Nov, 2019 **Visiting Student** **Weizmann Institute of Science, Israel**  
Introduction to cryo-focused ion beam SEM and consequent data processing.
- May, 2017 – Jun, 2018 **Visiting Student** **Weizmann Institute of Science, Israel**  
Training for sample preparation using high-pressure freezing and corresponding cryo-SEM imaging. Introduction to transmission electron microscope control.
- Oct, 2015 – May, 2016 **Student Internship In Research** **Central European Institute of Technology, Czech Republic**  
3D reconstruction of protein structure using TEM tomography and single particle analysis.

## Education

### Postgraduate Studies

- 2014 – ongoing **Ph.D. in Physical Engineering** **Brno University of Technology, Czechia**  
**Title:** Quantitative Imaging in Low-voltage Scanning Transmission Electron Microscope.  
**Supervisor:** Dr. Vladislav Krzyzanek  
  
- 2013 – 2016 **M.Sc. in Biomedical Engineering and Bioinformatics** **Brno University of Technology, Czechia**  
**Title:** 3D Reconstruction of Macromolecular Complexes by Cryoelectron Microscopy.  
**Supervisor:** Dr. Daniel Nemecek  
  
- 2012 – 2014 **M.Sc. in Biophysics** **Masaryk University, Czechia**  
**Title:** Development and Characterization of Support Films for Quantitative Imaging Using a Scanning Transmission Electron Microscopy.  
**Supervisor:** Dr. Vladislav Krzyzanek  
  

### Undergraduate Study

- 2010 – 2013 **B.Sc. in Biomedical Engineering and Bioinformatics** **Brno University of Technology, Czechia**  
**Project Title:** Manifestation of Physiological Noise in fMRI Data.  
**Supervisors:** Dr. Martin Lamos
- 2009 – 2012 **B.Sc. in Medical Physics** **Masaryk University, Czechia**  
**Project Title:** Electron Microscopy on Biological Samples.  
**Supervisor:** associate professor Petr Mikulik

### Other Training

- Nov 2019 **Machine Learning Course** **Machine Learning College, Czechia**  
Main topics: introduction to machine learning, convolutional neural networks and image processing, time series.
- Oct 2019 **Autumn School of Electron Microscopy** **Institute of Scientific Instruments of the CAS, Czechia**  
Theoretical course with practical demonstrations dealing with the basics of SEM, ESEM, low-voltage (S)TEM and FIB-SEM.



## Skills

### Programming:

MATLAB	● ● ● ● ●
LabVIEW	● ● ● ● ●
Bash scripting	● ● ● ● ●
Python	● ● ● ● ●
iFAST	● ● ● ● ●

### Tools:

Autodesk Inventor	● ● ● ● ●
LaTeX	● ● ● ● ●
Bsoft	● ● ● ● ●
IMOD	● ● ● ● ●
Relion	● ● ● ● ●

### Monte Carlo simulation:

CASINO	● ● ● ● ●
MONCA	● ● ● ● ●

## Profiles



## Memberships



## Personal

Radim lives with his wife, an accountant, their two daughters, born November 2017 and August 2019. In addition to taking care of his daughters he likes MTB, hiking, via ferrata, canoeing, model construction and history of ancient Rome. He is volunteer in Junák - Czech Scout with leadership exams.

## References

Ref. 1 Dr. Vladislav Krzyzanek, ISI CAS, Czechia, krzyzanek[at]isibrno.cz

Ref. 2 Dr. Eyal Shimoni, WIS, Israel, shimoni.eyal[at]gmail.com

Ref. 3 Dr. Jana Nebesarova, Biology Centre CAS, Czechia, nebe[at]paru.cas.cz

## Honours and Awards

Sep 2019	Best Oral Presentation Award	Beograd, Serbia
Sep 2017	Grant of the ThermoFisher Scientific and the Czechoslovak Microscopy Society	Lednice, Czechia
2011-2018	Awarded M.Sc. and Ph.D. Scholarships	Brno, Czechia

## Invited Talks

Nov 2019	<b>Biomedical signal analysis and processing for diagnostics workshop</b>	Institute of Physiology of the CAS
	Gave a half hour lecture on quantitative imaging in a SEM.	

## Publications

### Journals

- Abdolahpur Monikh, F., ... **Skoupy, R.**, ... Engineered Nanoselenium Supplemented Fish Diet: Toxicity Comparison with Ionic Selenium and Stability against Particle Dissolution, Aggregation and Release. *Environmental Science: Nano*, (2020).
- Skoupy, R.**, Fort, T., Krzyzanek, V. Nanoscale Estimation of Coating Thickness on Substrates via Standardless BSE Detector Calibration. *Nanomaterials* 10 (2020), 332.
- Turanek Knotigova, P., ... **Skoupy, R.**, ... Application of Advanced Microscopic Methods to Study the Interaction of Carboxylated Fluorescent Nanodiamonds with Membrane Structures in THP-1 Cells: Activation of Inflammasome NLRP3 as the Result of Lysosome Destabilization. *Molecular Pharmaceutics* 16- 8 (2019) 3441–3451.
- Drazanova, E., Kratka, L., Vaskovicova, N., **Skoupy, R.**, ... Olanzapine exposure diminishes perfusion and decreases volume of sensorimotor cortex in rats, *Pharmacol. Reports*. 71 (2019) 839–847.
- Skoupy, R.**, Nebesarova, J., Slouf, M., Krzyzanek, V. Quantitative STEM imaging of electron beam induced mass loss of epoxy resin sections, *Ultramicroscopy* 202 (2019) 44-50.
- Holan, V., ... **Skoupy, R.**, ... A murine model of the effects of inhaled CuO nanoparticles on cells of innate and adaptive immunity – a kinetic study of a continuous threemonth exposure, *Nanotoxicology* (2019).
- Marvanova, S., Kulich, P., **Skoupy, R.**, ... Size-segregated urban aerosol characterization by electron microscopy and dynamic light scattering and influence of sample preparation, *Atmos. Environ.* 178 (2018) 181–190.
- Fialova, D., **Skoupy, R.**, Drozdova, E., ... The Application of Scanning Electron Microscopy with Energy-Dispersive X-Ray Spectroscopy (SEM-EDX) in Ancient Dental Calculus for the Reconstruction of Human Habits, *Microsc. Microanal.* 23 (2017) 1207– 1213.

### Conferences

- M&M 2020 [online] - Beam energy dependent calibration of STEM and BSE detectors for thin film thickness estimation - talk
- MCM Belgrade 2019, Serbia - Assessing the thickness error rate of quantitative STEM measurements - talk
- IMC Sydney 2018, Australia - Correlative cryo-qSTEM-CL imaging in a SEM - poster
- NANOCON Brno 2018, Czechia - Determination of thickness refinement using STEM detector segments - poster
- MCM Rovinj 2017, Croatia - Soil contamination of human dental calculus determined by EDS - talk
- ISM Rehovot 2017, Israel - Cathodoluminescence imaging and mapping of biological samples in cryoSEM - poster
- EMC Lyon 2016, France - Plasma cleaning effect on the stability of the Epon resin sections - poster
- MMC Eger 2015, Hungary - Electron beam induced mass loss dependence on aging of epon resin sections - talk

# Abstract

This thesis deals with the possibilities of quantitative imaging in scanning (transmission) electron microscope (S|T|EM) together with its correlative applications. It starts with quantitative STEM (qSTEM) method description, where estimated local sample thickness can be related to irradiated dose and create a mass-loss study, which was applied on samples of ultra-thin epoxy resin sections at variate conditions (age, temperature, staining, plasma cleaning, carbon covering, probe current). The possibilities of the detector calibration process, the necessary background of the Monte Carlo simulations of electron scattering and achievable accuracy of the method are discussed and demonstrated. The method is then extrapolated for the use of back-scattered electron (BSE) detector, where new detector calibration technique, based on primary beam deflection on electron mirror, was postulated, developed and tested on various thin coating layers with thicknesses in range from 1 to 25 nm. The use of BSE detector brings the opportunity to measure the thickness of not only the electron transparent samples as in case of qSTEM, but also thin layers on substrates – qBSE. Both above-mentioned methods (qSTEM and qBSE) are intensity-based. This brings complication in the need of proper calibration, where just a slight drift of base-signal level causes a significant change of the results. This insufficiency was overcome in case of qSTEM by using the most probable scattering angle (captured by pixelated STEM detector) instead of an integral image intensity captured by an annular segment of STEM detector. The advantage of this method is its applicability post-acquisition, where no special previous actions are needed before each imaging session. The disadvantage is the limited range of detectable thicknesses given by the peak creation in signal/scattering-angle dependency. In general, low thickness region is immeasurable as well as those too thick (usable thickness range for latex is  $\sim 185$ -1,000 nm; given by detection geometry and pixel size). Moreover, multiple applications of conventional and commercially available quantitative techniques of cathodoluminescence (CL) and energy-dispersive X-ray spectroscopy (EDX) are presented in correlation with high-resolution images taken in secondary and transmitted electrons.